Mon. Not. R. Astron. Soc. **339,** 1041–1047 (2003)

Modelling enhanced density shells in the circumstellar envelope of IRC +10216

J. M. Brown[1]★ and T. J. Millar[2]†
[1]*Swarthmore College, Swarthmore, PA 19081, USA*
[2]*Department of Physics, UMIST, PO Box 88, Manchester M60 1QD*

Accepted 2002 November 4. Received 2002 November 4; in original form 2002 October 7

ABSTRACT

The circumstellar envelopes of very evolved, late-type asymptotic giant branch stars exhibit complex molecular structure. The most striking of these objects is the carbon star IRC +10216 (CW Leo), where over 50 molecular species, including carbon chains with up to nine carbon atoms, have been detected. The envelope of IRC +10216 is now known to contain dust shells of enhanced density which are well correlated with molecular shells seen in interferometric observations. The inclusion of shells, based on observed parameters, into a chemical model allows observations to be matched more closely. Another effect of enhanced density shells is the narrowing of the radii over which the peak abundances occur. Previous models tended to have the molecules spread over a larger band of radii than observations indicated. Thus, the effects of enhanced density shells are extremely important for understanding the circumstellar environments of stars such as IRC +10216.

Key words: molecular data – molecular processes – circumstellar matter – stars: individual: IRC +10216 – ISM: molecules.

1 INTRODUCTION

The chemistry of the carbon-rich asymptotic giant branch (AGB) star IRC +10216 is fascinatingly complex. The star has a large circumstellar envelope due to its high mass-loss rate, $\dot{M}$, which is thought to be greater than 10^{-5} $M_{\odot}$ yr^{-1} (Knapp & Morris 1985). This wind drives parent molecules from the star and, as the wind becomes more optically thin to external ultraviolet (UV) radiation from the interstellar medium, photochemistry creates reactive species which then undergo further chemical reactions. The region of the envelope where this chemistry can occur is limited because, while a certain amount of UV radiation is needed to drive the initial photochemistry, too much causes the molecules to dissociate rapidly to atoms and atomic ions. Modelling the abundances of various molecules in this region, followed by comparison with observations of these molecular abundances, helps probe the validity of current theories for the formation of these chemically rich shells and the formation of circumstellar molecules in general.

The diversity of molecules present in the envelope of IRC +10216 and its proximity to Earth have made it a favourite object of study. Several models have been made of the chemistry. Millar, Herbst & Bettens (2000) produced the most comprehensive model, which included 3851 reactions involving 407 gas-phase species. However, none of the models have included the dust shells that were identified in optical images by Mauron & Huggins (1999). These dust shells have an effect on the distribution of the molecules due to two factors. First, the dust shells are more optically thick than the surrounding material and decrease the amount of UV light reaching the regions inside the shells. This reduces the photodissociation rates of parent molecules. Secondly, the dust shells could have been formed during periods of greater mass loss (i.e. increased wind particle density) from IRC +10216. In this case, the increase in mass loss would also imply an increase in the number density of the shells, reducing the collision time-scales for formation of daughter species.

Enhanced density shells due to stellar pulsations are known to surround oxygen-rich AGB stars. However, until recently, no evidence had been found for high-density shells around carbon-rich stars, although theoretically conditions should be right to create them. Thus, the discovery of high-density shells in the outer envelope of IRC +10216 by Mauron & Huggins (1999) in two *B*- and *V*-band photographs originally taken by Crabtree, McLaren & Christian (1987) was not unexpected. Previously, the rings were thought to be scattered Galactic light from a dust envelope. The shells occur in the photochemically active region. The shells are extremely thin, with thicknesses ranging from 0.5 to 3.0 arcsec (1.5×10^{15} to 9.3×10^{15} cm at a distance of 200 pc). Shells at larger radii tend to be thicker, indicating the presence of a small dispersion velocity. The spacing between shells is irregular. The mechanism for the formation of these shells is unknown, although the inner envelope is known

★Present address: Department of Astronomy, CalTech 105-24, 1201 East California Blvd., Pasadena, CA 91125, USA.
†E-mail: Tom.Millar@umist.ac.uk

Table 1. Initial fractional abundances of parent species with respect to $n(H_2)$.

Species	Initial abundance
C_2H_2	5.0×10^{-5}
CH_4	2.0×10^{-6}
H_2S	1.0×10^{-6}
HCN	8.0×10^{-6}
NH_3	2.0×10^{-6}
CO	6.0×10^{-4}
CS	4.0×10^{-6}
N_2	2.0×10^{-4}

to be subjected to shorter time-scale pulsations. Multiple pulsations could combine to form one dust shell by sequentially raising the temperature and the density (Fleischer, Gauger & Sedlmayr 1992). Other potential causes include a variable mass-loss rate or wind velocity. The complex structure seen in planetary nebulae, the final stage of AGB mass loss, suggests that variable mass loss and high-density shells are typical for AGB stars.

2 MODEL

The computer modelling program calculates the radial fractional abundances of 409 species (see table 4 of Millar et al. 2000, for a complete listing). A total of 3864 gas-phase reactions using these species are included in the rate file. The effect of self-shielding on the CO abundances is taken into account. The program assumes a spherically symmetrical envelope. Therefore, without loss of generality, the abundances can be calculated along only one radial direction. The underlying distribution is the $1/r^2$ distribution of molecular hydrogen. All initial abundances were set to zero apart from the parent species which are formed at smaller radii (see Table 1).

The major difference in this model is the inclusion of dust shells, which affect the transfer of UV radiation within the envelope. We adopt a model with m shells specified by inner and outer radii r_{s1} and r_{s2} (where $s = 1, \ldots, m$), respectively, and density enhancement (contrast) β, taken to be a constant for all shells. Consider a radial distance r and the line of sight from r at an angle θ to the radial direction which cuts the shells at distances l_{s1} and l_{s2}, where l measures the distance along this line of sight. Then the radial column density of hydrogen in this direction is given by

$$N(r, \theta) = \int_{l=0}^{\infty} n(l)\,\mathrm{d}l + \beta \sum_{s=1}^{m} \int_{l_{s1}}^{l_{s2}} n(l)\,\mathrm{d}l.$$

For a $1/r^2$ distribution, we can integrate this equation to find

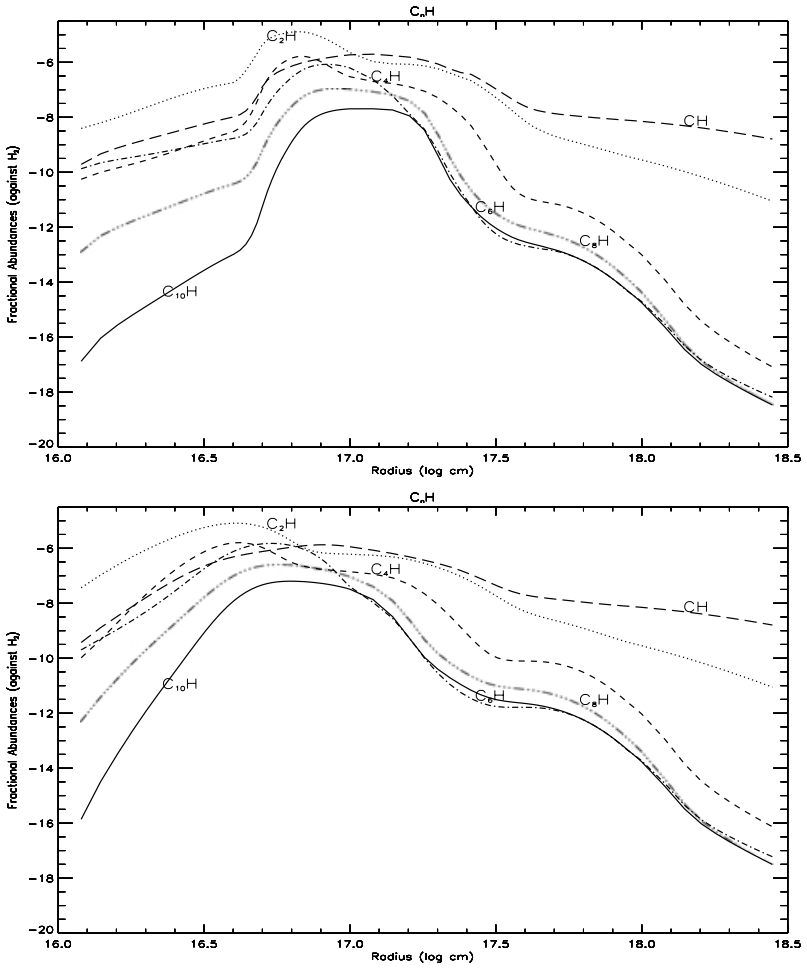

Figure 1. Comparison of C_nH group radial distributions for models with mass-loss rates of 3.0×10^{-5} $M_\odot$ yr^{-1}: (top) many rings (see Table 2) with a density enhancement (β) of 6.0; (bottom) no rings. Introduction of rings results in a significant narrowing of the molecular distributions. The high-density case produces a definite high-contrast ring of molecules, which should be clearly visible in molecular emission lines.

$$N(r,\theta) = N(r)\frac{\theta}{\sin\theta} + \frac{\beta N(r)}{\sin\theta} \times \sum_{s=1}^{m}\left[\tan^{-1}\left(\frac{r_{s2}^2}{r^2\sin^2\theta}-1\right)^{1/2} - \tan^{-1}\left(\frac{r_{s1}^2}{r^2\sin^2\theta}-1\right)^{1/2}\right]$$

where $N(r)$ is the column density of hydrogen in the radial direction from r to infinity. The column density $N(r,\theta)$ is used to determine the optical depth in the UV, $\tau(r,\theta)$, and hence the intensity of interstellar UV radiation, $I(r,\theta)$. Integration over angle then determines the UV flux, $I(r)$, at radial distance r. We note that the above analysis is correct when the radial distance r is less than the radial distance of the innermost shell. When this is not the case, a more careful treatment is needed as the line of sight may cross a shell twice or miss a shell entirely. We have implemented this in our numerical calculations.

We have investigated a large number of models, varying the number, width, density contrast and positions of the shells. Here we present the results of a five-shell model based on the observations of Mauron & Huggins (2000), with shell thicknesses taken from their work. The shell parameters are given in Table 2. Lucas & Guélin (1999) have identified molecular emission structures on scales as small as 4 arcsec, much closer to the star than the photochemical shells discussed in this paper. These structures, which may be either shells or clumps, are seen predominantly in species such as the metal halides, HCN and SiS, all of which are thought to be produced by photospheric chemistry.

Table 2. Inner and outer radii of the shells, in units of 10^{17} cm.

Inner radius	Outer radius
0.389	0.495
0.598	0.615
1.32	1.47
1.59	1.74
2.24	2.39

3 RESULTS

The model was run using several sets of starting parameters to determine the effects of each one. Mass-loss rates of 3.0×10^{-5} $M_\odot$ yr^{-1} were mostly used, although several models using a mass-loss rate of 1.0×10^{-6} $M_\odot$ yr^{-1} were investigated but were found to be affected negligibly by the shells. Here we present

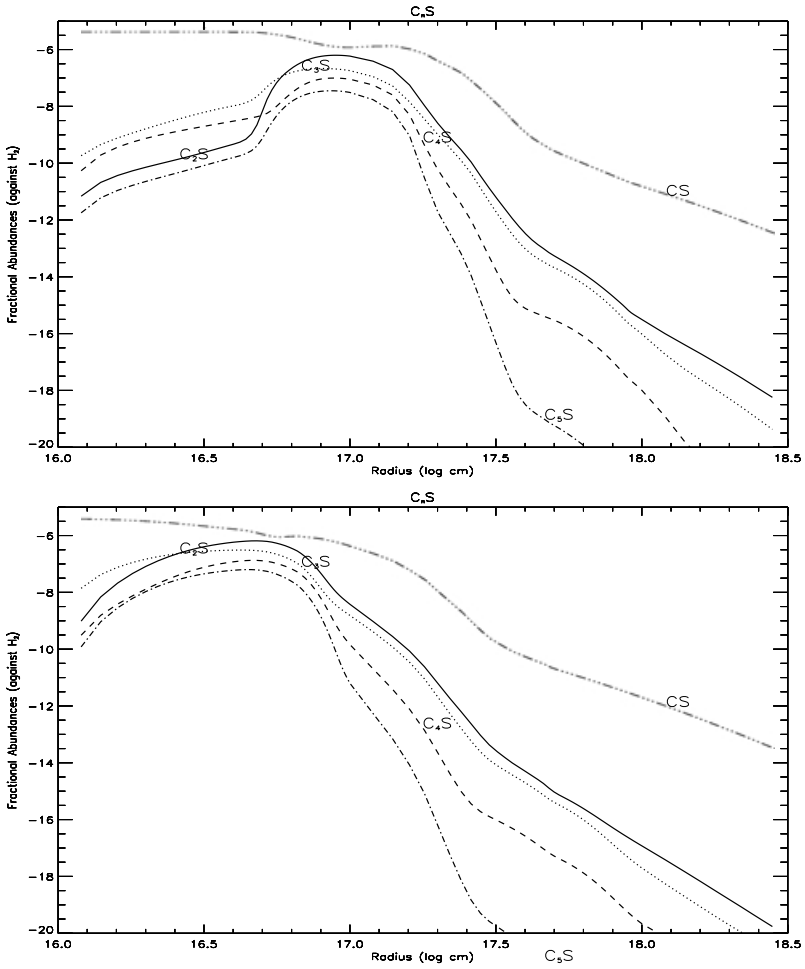

Figure 2. Comparison of C_nS group radial distributions for models with many rings (see Table 2) with density enhancements (β) of 6.0: (top) mass-loss rate of 3.0×10^{-5} $M_\odot$ yr^{-1}; (bottom) mass-loss rate of 1.0×10^{-5} $M_\odot$ yr^{-1}. As for the C_nH group, the higher mass-loss rate produces an extreme narrowing of the molecular distribution, demonstrating that this phenomenon is not limited to a particular subgroup of molecules. This behaviour is shown by all complex species.

the results of three models, for two different values of both the mass-loss rate $\dot{M}$ and the density enhancement β:

(1) $\dot{M} = 3.0 \times 10^{-5}$ $M_\odot$ yr^{-1} and $\beta = 3$;
(2) $\dot{M} = 3.0 \times 10^{-5}$ $M_\odot$ yr^{-1} and $\beta = 6$;
(3) $\dot{M} = 2.0 \times 10^{-5}$ $M_\odot$ yr^{-1} and $\beta = 6$.

Note that, even with a density enhancement of 6, the average mass-loss rate increases by only about 10 per cent.

Obviously, larger density enhancements produce greater changes than smaller ones. The exact enhancement in the shells is unknown, although 6 is at the high end of the estimated range and 3 is more likely (Mauron & Huggins 2000). Single shells had small effects but the greatest changes in distribution occurred with multiple shells. The shells at 6.0×10^{16} and 1.3×10^{17} cm had the greatest effects since they were just outside of the region of highest chemical activity. The exact position and density enhancement of these two shells can radically change the chemical abundances and distributions in the circumstellar envelope.

Several variables were examined for their effect on the distribution of the molecules in IRC +10216. These were placement and width of the rings, mass-loss rates and degree of density enhancement. The rings are based on a multiplication of the underlying density of the envelope, which follows a $1/r^2$ distribution. Thus, the outer rings are less dense while still maintaining the same contrast to the surrounding material. According to Mauron & Huggins (1999), this is probably not accurate as images indicate that the density contrasts are larger closer to the centre of the star before dispersion can occur. However, the dispersion velocity is small enough, ~0.7 km s^{-1}, that this approximation is valid (Mauron & Huggins 2000).

Regardless of mass-loss rate, the rings just outside of the areas of peak abundance appear to have the most effect. At a mass-loss rate of 3.0×10^{-5} $M_\odot$ yr^{-1}, the highest abundances of daughter products occur, for a smooth density distribution, at around 5.0×10^{16} cm so that rings near 1.0×10^{17} cm are able to alter significantly the radial distributions of molecular abundances. Single shells produce mainly local effects as well as small continuous deviations at all radii within the shell. Shells that are much beyond the photodissociation region do provide additional extinction but the effect is generally small as the densities of these shells are lower than those at smaller radii. At radii smaller than the photodissociation region, the additional blocking of UV light by the shells reduces the photodissociation rates of parent species and delays the growth in abundance of daughter species.

The mass-loss rate controls the position and size of the region of photoactivated chemical processes. Increasing the mass-loss rate shifts the chemically active regions to slightly greater radii, but does

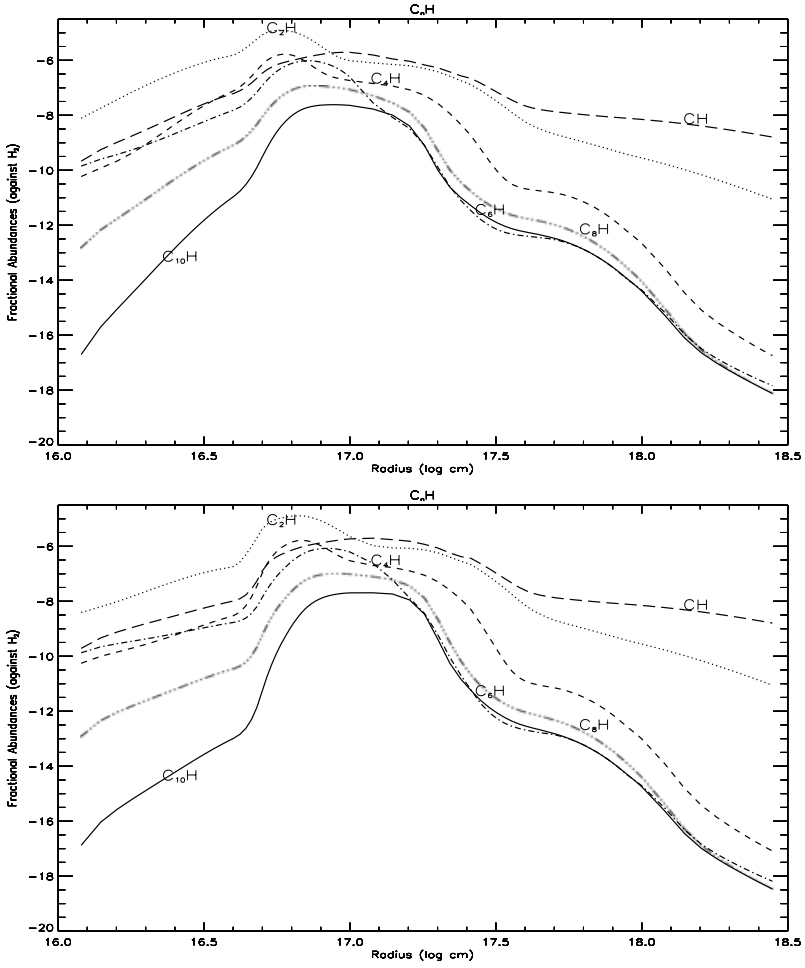

Figure 3. Comparison of C_nH group radial distributions for models with many rings and mass-loss rates of 3.0×10^{-5} $M_\odot$ yr^{-1}: (top) density enhancement of 3.0; (bottom) density enhancement of 6.0. The change in density enhancement results in no change in the position of the peak abundances. The higher density enhancement produces steep decreases in abundance below the critical radius of 6.0×10^{16} cm, where the UV radiation is too weak to activate many chemical reactions.

not result in any dramatic change in the shape of the radial distributions. The higher mass-loss rate (3.0×10^{-5} $M_\odot$ yr^{-1}) produces an extreme narrowing of the molecular distribution since the additional density makes the stellar wind more opaque, resulting in an outward shift of the radius of the initial chemical activity (Fig. 1). The lower mass-loss rates (1.0 and 2.0×10^{-5} $M_\odot$ yr^{-1}), while having the same trends, have less dramatic results (Fig. 2). However, models with mass-loss rates below 1.0×10^{-5} $M_\odot$ yr^{-1} show little effect from the addition of rings, even with high density enhancements of up to a factor of 6 and the presence of rings within the high-abundance region. This effect, which occurs for all molecules and is thus a global trend, is due to the fact that the optical depth in the envelope is now so low that the photochemistry is driven at a very small radial distance so that the addition of shells much further out, and at relatively low density, does not provide any significant additional extinction.

Larger density enhancements obviously have greater impact on the molecular distribution. Changes in density enhancement for the same mass-loss models result in no change in the position of the peak abundances. The higher density enhancement (6.0) produces steep decreases in abundance inside the ring where the UV radiation is too weak to activate the photochemistry (Fig. 3).

4 DISCUSSION

Agreement with observation is essential to verify this model. There are three conditions that the model must fulfil: any observed carbon-based molecules must be predicted by the model; column densities for each molecule should be in agreement with observations; and the spatial location of the molecules should agree with observations in both position and width.

Over 50 molecules have been detected in the envelopes of carbon-rich AGB stars. Molecules containing metals including silicon and magnesium have been omitted from this model since these compounds are seen only close to the star and are likely to be depleted due to incorporation of metals into dust grains at inner radii.

Radial column densities for our models agree with observations within reasonable limits (see Table 3), although they are slightly lower in all cases, with the exception of C_3H, than the results of Millar et al. (2000). The chemical reaction network used here is similar to that of Millar et al. (2000) but more complex than those of Millar & Herbst (1994) and Doty & Leung (1998). Similar parameters for the star were used, including mass-loss rate and wind velocity.

Many recent advances have been made in observing molecules in the millimetre and submillimetre wavelengths. Guélin et al. (2000) found that HCO^+, C_2H, C_4H, HC_5N and $HC^{13}CCN$ all occur in the same region around the star between 10 and 18 arcsec (i.e. between 3.0 and 5.5×10^{16} cm at a distance of 200 pc) (see Fig. 4). The spatial location of the molecules agrees with observation for a mass-loss rate between 2 and 3×10^{-5} $M_\odot$ yr^{-1}. The alignments of the peak abundances (fractional abundance with respect to H_2 of 10^{-6} or greater) seen in the maps do not correspond well with models without enhanced density shells. However, the presence of the shells restricts the molecules to a narrow range of radial distances and increases observational agreement (see Fig. 4). The spatial alignment of the molecules indicates that they form quasi-simultaneously, within 150 yr (Guélin et al. 2000). This simultaneous formation is difficult to achieve in models without the presence of high-density shells due to the high mass-loss rate. The shells confine the chemically active region, leading to simultaneous formation and thus a narrower molecular shell.

Table 3. Comparison of observed and calculated column densities. Models (1) to (3) are described in the text.

		Calculated			Other work[a]	
Species	Observed (ref.[a])	Model (1)	Model (2)	Model (3)	MHB	MH	DL(C)
C	1.1E+16 (1)	9.3E+15	7.6E+15	8.3E+15	1.0E+16	2.7E+16	1.3E+16
C_3	1E+15 (2)	5.6E+14	5.0E+14	5.4E+14	6.5E+14	4.7E+14	3.1E+14
C_5	1E+14 (3)	4.0E+14	3.1E+14	4.6E+14	7.5E+14	1.1E+15	9.6E+13
C_2H	3-5E+15 (4,5,6)	3.6E+15	3.3E+15	4.7E+15	5.7E+15	1.8E+16	7.7E+15
C_3H	3E+13 (4,7)	2.4E+14	2.1E+14	3.3E+14	1.4E+14	1.4E+14	2.1E+14
C_4H	2-9E+15 (4,6,7,8)	3.7E+14	3.2E+14	6.0E+14	1.0E+15	5.5E+15	4.7E+14
C_5H	2-50E+13 (4,7)	7.5E+13	6.6E+13	1.1E+14	8.7E+13	5.5E+13	3.5E+13
C_6H	3-30E+13 (4,7)	2.1E+14	1.7E+14	4.0E+14	5.8E+14	4.5E+14	8.2E+13
C_7H	1E+12 (4)	2.1E+13	1.8E+13	3.6E+13	4.5E+13	5.4E+12	3.8E+13
C_8H	5E+12 (4)	3.3E+13	2.6E+13	6.6E+13	1.1E+14	3.6E+13	4.0E+12
C_3H_2	2E+13 (7)	1.8E+13	1.7E+13	1.7E+13	2.1E+13	3.0E+13	7.0E+13
C_4H_2	3-20E+12 (7,9)	1.5E+15	6.7E+14	2.2E+15	2.9E+15	4.7E+15	8.6E+14
C_3N	2-4E+14 (7,10)	1.5E+14	1.3E+14	2.3E+14	3.2E+14	2.2E+14	1.9E+14
C_5N	3E+12 (10)	4.3E+13	3.4E+13	7.3E+13	1.4E+14	2.3E+14	6.4E+13
HC_3N	1-2E+15 (7,10)	9.2E+14	5.3E+14	1.4E+15	1.8E+15	2.8E+15	1.4E+15
HC_5N	2-3E+14 (7,10)	1.9E+14	1.3E+14	4.5E+14	7.1E+14	1.2E+15	1.1E+14
HC_7N	1E+14 (7)	5.5E+13	3.8E+13	1.6E+14	2.2E+14	2.6E+14	7.8E+12
HC_9N	3E+13 (7)	1.4E+13	9.4E+12	4.9E+13	5.8E+13	5.1E+13	3.8E+12
HCO^+	3E+12 (11)	1.6E+12	1.7E+12	1.3E+12	2.4E+12		
CH_3CN	6E+12 (12)	2.4E+12	2.6E+12	2.8E+12	3.4E+12		

[a]References: MHB, Millar et al. (2000); MH, Millar & Herbst (1994); DL(C), model C of Doty & Leung (1998); 1, Keene et al. (1993); 2, Hinkle, Keady & Bernath (1988); 3, Bernath, Hinkle & Keady (1989); 4, Guélin et al. (1997); 5, Groesbeck, Phillips & Blake (1994); 6, Avery et al. (1992); 7, Kawaguchi et al. (1995); 8, Dayal & Bieging (1993); 9, Cernicharo et al. (1991); 10, Guélin, Neininger & Cernicharo (1998); 11, Olofsson (1997); 12, Guélin & Cernicharo (1991).

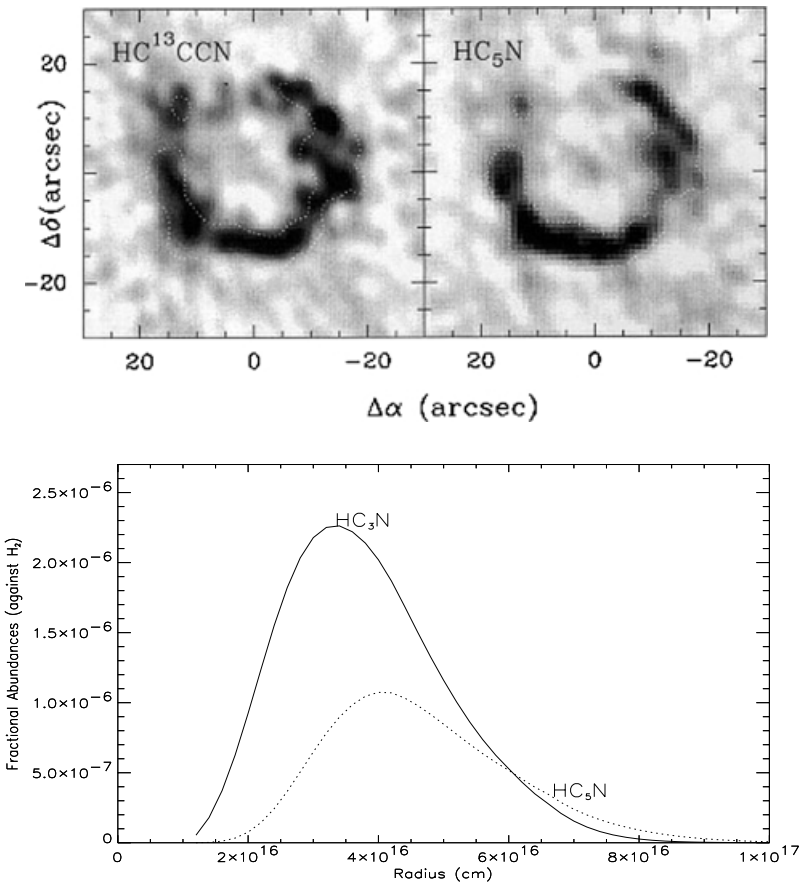

Figure 4. (top) The distribution of $HC^{13}CCN$ and HC_5N as seen at a wavelength of 3 mm (Guélin et al. 2000). (bottom) Model with a mass-loss rate of 2.0×10^{-5} $M_\odot$ yr^{-1} and a density enhancement (β) of 6.0. Unlike all other plots, radius and fractional abundance are plotted on a linear rather than logarithmic scale to allow better comparison. Radius value 2.0×10^{16} cm is equivalent to 6.5 arcsec, 4.0×10^{16} cm is equivalent to 13 arcsec, and 6.0×10^{16} cm is equivalent to 20 arcsec. The alignment between model and observation is good for both molecules. HC_5N also peaks at a slightly larger radius than HC_3N in both the model and the image. The width of the molecular shell is around 2.5×10^{16} cm for both.

5 CONCLUSIONS

The circumstellar envelope of the carbon-rich AGB star IRC +10216 is now known to contain shells of enhanced density. Enhanced density shells, based on the properties of those observed, were added to the existing chemical model of Millar et al. (2000). Spherical shells with different positions, widths and density enhancements were examined to determine the effects of each property. Different mass-loss rates were also examined. We find that the addition of shells does not have any significant effect when the mass-loss rate is low – the amount of additional material is too small to alter the intensity of UV radiation appreciably – but is important when the mass-loss rate is large. In this case, the shells change the molecular distributions in the circumstellar envelope. In general, the chemically active region narrows and moves slightly outwards upon addition of enhanced density shells since activating UV radiation does not reach the inner regions of the envelope as effectively and species in the outer envelope have an increased shielding due to the extra material contained in the shells. This narrowing is particularly evident when a dust shell lies just outside the region where parents are photodissociated in the envelope.

Multiple high-density shells, which provide the largest effects, produce a definite high-contrast ring of molecules, which should be clearly visible in molecular emission lines. New millimetre observations of HCO^+, C_2H, C_4H and HC_5N reveal this structure (Guélin et al. 2000) and are well correlated with those predicted by the models.

This study of the effects of high-density shells on molecular distribution could be continued in several directions, particularly to O-rich AGB stars and protoplanetary nebulae. Modelling of these objects could provide a broader view of the evolution of the shells as the star ages. There is also much observational work to be done in this field to detect more molecules and further to establish the shell structure and its temporal evolution.

ACKNOWLEDGMENTS

Astrophysics at UMIST is supported by a grant from PPARC. JMB is glad to acknowledge financial support from Sigma Xi Research Society. JMB would also like to thank UMIST for their hospitality and Swarthmore College Department of Physics and Astronomy for their support throughout this project.

REFERENCES

Avery L. W. et al., 1992, ApJS, 83, 363
Bernath P. F., Hinkle K. H., Keady J. J., 1989, Sci, 244, 562
Cernicharo J., Gottlieb C. A., Guélin M., Killian T. C., Thaddeus P., Vrtilek J. M., 1991, ApJ, 368, L43

Crabtree D. R., McLaren R. A., Christian C. A., 1987, in Kwok S., Pottasch S. P., eds, Late Stages of Stellar Evolution. Reidel, Dordrecht, p. 145
Dayal A., Bieging J. H., 1993, ApJ, 407, L37
Doty S. D., Leung C. M., 1998, ApJ, 502, 898
Fleischer A. J., Gauger A., Sedlmayr E., 1992, A&A, 266, 321
Groesbeck T. D., Phillips T. G., Blake G. A., 1994, ApJS, 94, 147
Guélin M., Cernicharo J., 1991, A&A, 244, L21
Guélin M. et al., 1997, A&A, 317, L1
Guélin M., Neininger N., Cernicharo J., 1998, A&A, 335, L1
Guélin M., Lucas R., Neri R., Bremer M., Broguiere D., 2000, in Minh Y. C., van Dishoeck E. F., eds, Proc. IAU Symp. 197, Astrochemistry: From Molecular Clouds to Planetary Systems. Sheridan Books, Chelsea, MI, p. 365
Hinkle K. H., Keady J. J., Bernath P. F., 1988, Sci, 241, 1319
Kawaguchi K., Kasai Y., Ishikawa S., Kaifu N., 1995, PASJ, 47, 853
Keene J., Young K., Phillips T. G., Buttgenbach T. H., 1993, ApJ, 415, L131
Knapp G. R., Morris M., 1985, ApJ, 292, 640
Lucas R., Guélin M., 1999, in Le Bertre T., Lebre A., Waelkens C., eds, Proc. IAU Symp. 191, Asymptotic Giant Branch Stars. Astron. Soc. Pac., San Francisco, p. 305
Mauron N., Huggins P. J., 1999, A&A, 349, 203
Mauron N., Huggins P. J., 2000, A&A, 359, 707
Millar T. J., Herbst E., 1994, A&A, 288, 561
Millar T. J., Herbst E., Bettens R. P. A., 2000, MNRAS, 316, 195
Olofsson H., 1997, in van Dishoeck E. F., ed., Molecules in Astrophysics, Probes and Processes. Kluwer, Dordrecht, p. 457

This paper has been typeset from a TEX/LATEX file prepared by the author.